

Investigating Fault-Sealing Effects on Induced Seismicity and Pore Pressure Distribution in Northeastern British Columbia (Parts of NTS 093P, 094A): Observations

Z. Esmailzadeh¹, Department of Geoscience, University of Calgary, Calgary, Alberta, zahra.esmailzadeh@ucalgary.ca

D.W. Eaton, Department of Geoscience, University of Calgary, Calgary, Alberta

Esmailzadeh, Z. and Eaton, D.W. (2022): Investigating fault-sealing effects on induced seismicity and pore pressure distribution in northeastern British Columbia (parts of NTS 093P, 094A): observations; *in* Geoscience BC Summary of Activities 2021: Energy and Water, Geoscience BC, Report 2022-02, p. 49–60.

Introduction

The Montney shale gas play in northeastern British Columbia (BC) contains overpressured terranes, which preserve the signature of elevated formation pressures that formed during hydrocarbon migration near the time of maximum burial. The spatially varying pattern of overpressure signatures is thought to reflect loss of pressure along permeable fairways, such as faults, during uplift and exhumation. Other studies, however, show that distinct pressure terranes within the Montney play are likely fault bounded, implying that some faults continue to serve as seals that inhibit pressure migration. These two concepts can be reconciled within the framework of the fault-valve model, wherein a fault experiences a transient coseismic increase in permeability during an earthquake. According to this model, the fault seal rebuilds gradually over time during the ensuing interseismic period, such that complete release of overpressure within a fault-bounded compartment may require multiple fault activation cycles.

A local magnitude (M_L) 4.5 hydraulic-fracturing (HF) induced earthquake on November 30, 2018, and the ensuing seismicity sequence, occurred close to a major pressure boundary within the Septimus oil and gas field and surrounding area. The sequence was triggered by HF treatment in two horizontal wells, in the Lower–Middle Montney members, which straddled a major pressure boundary. Pressure readings from these wells show that the lateral pressure difference across the boundary was approximately 10 megapascals (MPa) over a distance <2.3 km, and provided evidence for a coseismic pressure drop of about 3 MPa. This paper reviews the available data from this area, with the objective of reappraising pressure terrane boundaries in light of recently mapped structural corridors, and evaluating the relationship between structural corridors,

pressure terranes and log-derived geomechanical parameters. The study area encompasses the Septimus field, including the location of the November 2018 earthquakes, and covers a large part of the Kiskatinaw Seismic Monitoring and Mitigation Area (KSMMA; Figure 1). The datasets that have been compiled within this study area are summarized in Table 1.

Structural Corridors

The Western Canada Sedimentary Basin (WCSB) is a mature oil and gas basin with an extraordinary endowment of publicly accessible data. The basin contains structural elements of varying age, expressed as folding, faulting and fracturing, which provide a record of tectonic activity during basin evolution (Wozniakowska et al., in press). In a region of the WCSB, straddling the border between Alberta and BC and covering an area of approximately 130 000 km², Wozniakowska et al. (in press) used publicly available fault data, formation top data, LITHO-PROBE seismic profiles and regional potential-field data to delineate regional structural elements. They adopted a structural-corridor approach, which helps to resolve the limited spatial extent of available seismic data and provides broader spatial coverage, enabling the investigation of structural trends throughout the entirety of the Montney play (Wozniakowska et al., in press). In this study, pressure terranes (Fox and Watson, 2019; Enlighten Geoscience Ltd., 2021) and property discontinuities are compared with these structural corridors (Figure 2a, b). As summarized in Table 2, these two independent interpretations correlate strongly within and/or at the boundaries of the Septimus High, Wilder Moderate (Mod.) High–Cecil Low and Wilder Mod. High–Monias Low pressure terranes.

Pore Pressure and Stress Mapping

The hydrogeological setting is considered one of the most important considerations in understanding induced seismicity (Fox and Watson, 2019). In very low permeability plays, structural features can cause significant pressure

¹The lead author is a 2021 Geoscience BC Scholarship recipient.

This publication is also available, free of charge, as colour digital files in Adobe Acrobat® PDF format from the Geoscience BC website: <http://geosciencebc.com/updates/summary-of-activities/>.

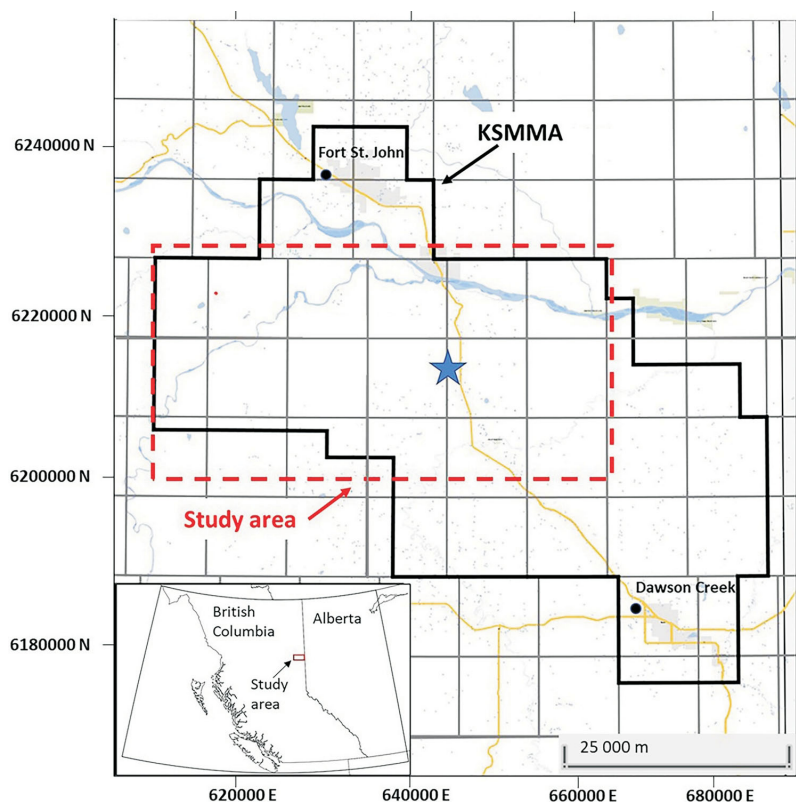


Figure 1. Location of the study area (red dashed outline) and Kiskatinaw Seismic Monitoring and Mitigation Area (KSMMA; black outline) in northeastern British Columbia. The star shows the approximate location of the November 30, 2018, earthquake sequence. All co-ordinates are in UTM Zone 10 North, NAD 83.

Table 1. List of data compiled for this study area, northeastern British Columbia. Well data and reservoir parameters were provided by geoLOGIC systems ltd. © 2021, seismic events from Visser et al. (2017) and Salvage and Eaton (2021) and structural corridor shapefiles from Wozniakowska et al. (in press). Abbreviations: N/a, not available; PVT, pressure-volume-temperature.

Data	Number of wells/ amount of data analyzed	Formation
Formation tops	8000	Debolt to Shaftesbury
Advanced core analysis	20	Montney
Fluid and PVT data	10	Montney
Production/injection data	1500	Montney
Diagnostic fracture injection test (DFIT)	149	Montney
Well logs	111	Debolt to Shaftesbury
Pressure data	1600	Debolt to Halfway
Well surveys	224	N/a
Seismic events	3639	N/a
Structural corridor shapefiles	134	N/a

compartmentalization (Fox and Watson, 2019; Wood et al., 2021). Pressure gradient maps of the Upper and Middle Montney members from Fox and Watson (2019) are shown in Figure 3a and b. The figure shows several transitions across the study area from relatively high (>14 kPa/m) to low (<10 kPa/m) pressure gradient values. The epicentral region of the November 30, 2018, earthquake sequence seems to correlate with a sharp contrast in lateral pore pressure in the Montney Formation.

To validate and update these results, Montney Formation pore pressure data were extracted from diagnostic fracture injection tests (DFITs) and routine pressure survey tests (PST). All tests were subjected to quality control (QC) evaluation to remove poor quality tests, to account for different gauge resolutions and to exclude the outliers. Pressure data with less than 10 days of shut-in duration were ignored. For individual wells, the pressure data were extrapolated to the initial reservoir pressure. For the Montney Formation, most of the pressure data are within the Upper Montney Member and the least amount of data are within the Lower Montney Member. The PST data include tests from the following categories: pressure gauge fall-off (PGFO), pressure gauge build-up (PGBU) and static gradient (SG). All of these tests were reviewed to ensure the best possible pressure value for each tested interval was included in the final maps. Figure 4 shows different ranges of pressure gradient in the Montney Formation measured with different tools. Since the mean value of all the methods are close and they all cover similar ranges of data, down-hole gauge pressure (PGFO, PGBU, SG) and DFIT data were used confidently. Due to limitations in memory and runtime for this model, only the pressure data from the wells with full-set logs (111 wells) were considered.

Diagnostic fracture injection tests, also known as minifrac tests, include a short injection test followed by a few hours of fall-off. During the injection, the rock formation breaks down to allow wellbore communication past the damage zone. The post-shut-in pressure decay is used to estimate reservoir parameters needed for fracture design. Interpretation of DFIT results provides estimates of reservoir pore pressure, fracture pressure, fracture closure pressure (approximately equivalent to minimum horizontal stress), permeability and rock elastic parameters, such as Young's modulus. In addition, the flow regime is identified to confirm the reservoir parameters. In this study, DFIT interpretation reports were available for 149 wells.

Within the Montney Formation, areas with strong lateral gradients in pore pressure appear to mark the locations of faults that bound pressure compartments and coincide with zones that appear to be more prone to induced seismicity.

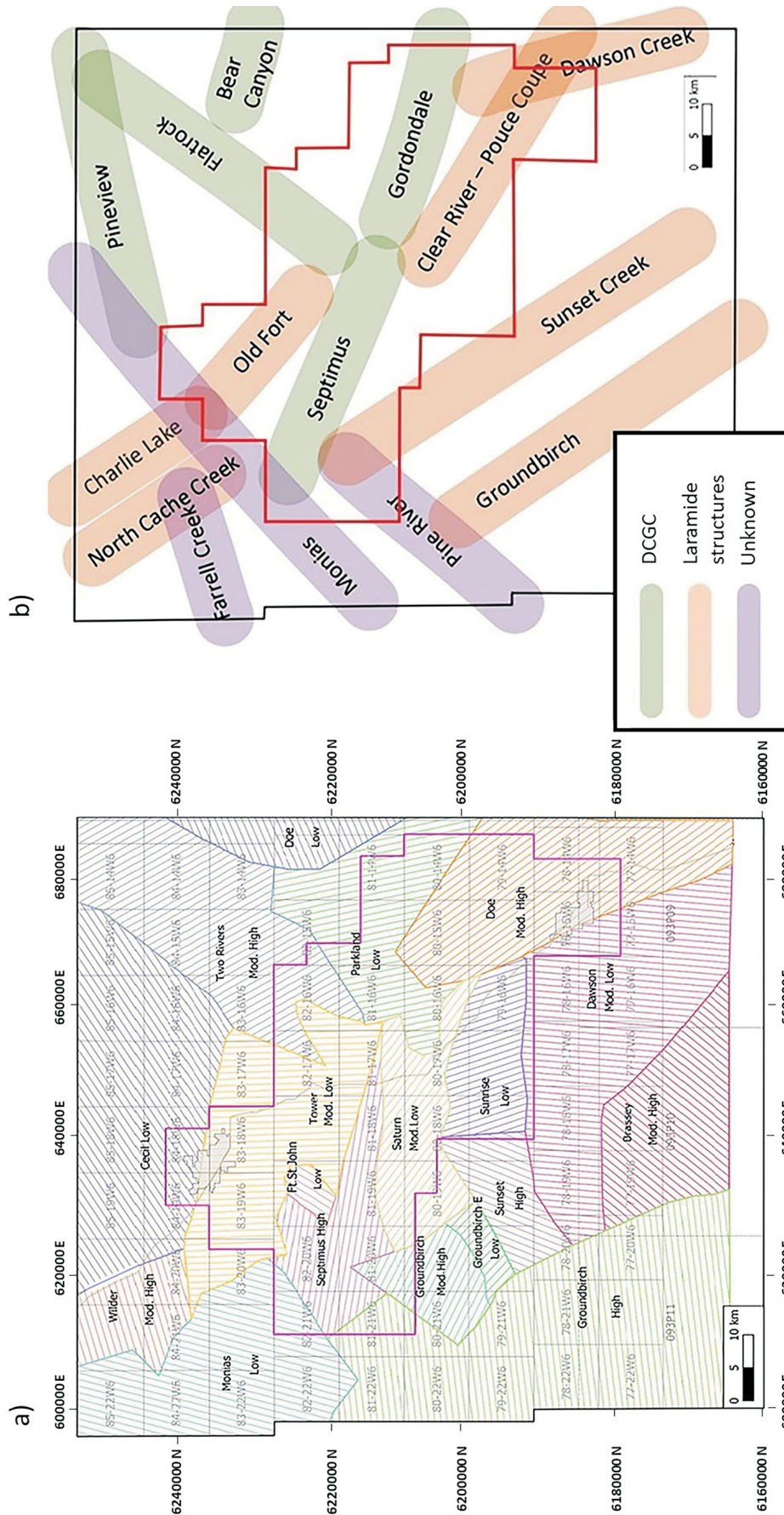


Figure 2. Comparison between **a)** pressure terranes (modified from Fox and Watson, 2019) and **b)** structural corridors (modified from Wozniakowska et al., in press), northeastern British Columbia. Some NTS map numbers (e.g., 093P11) and townships and ranges are noted in the background (e.g., 77-22W6, Twp. 77, Rge. 22, W 6th Mer.). All co-ordinates are in UTM Zone 10 North, NAD 83. Abbreviations: DCGC, Dawson Creek graben complex; E, east; Mod., moderate.

Table 2. Comparative summary of structural corridors and pressure terranes in the study area, northeastern British Columbia (see Figure 2). Abbreviations: Mod., moderate; N/a, not applicable.

Structural corridor	Pressure terrane	Degree of correlation
Septimus	Septimus High	Very high
Charlie Lake	Wilder Mod. High–Cecil Low	Very high
North Cache Creek	Wilder Mod. High–Monias Low	Very high
Dawson Creek	Doe Mod. High–Dawson Mod. Low	High
Groundbirch	Groundbirch High–various Lows	High
Old Fort	Septimus High–Ft. St. John Low	Partial
Flatrock	Two Rivers Mod. High	Partial
Monias	Septimus High–Monias Low	Partial
Clear River – Pouce Coupe	Saturn Mod. Low–Sunrise Low	Partial
Pine River	Groundbirch High	Partial
Bear Canyon	Two Rivers Mod. High–Parkland Low	Partial
Gordondale	N/a	None
Pineview	N/a	None
Farrell Creek	N/a	None
Sunset Creek	N/a	None

The epicentre of the M_L 4.5 event on November 30, 2018, also corresponds to an area with significant lateral pore pressure variation at the Montney Formation level. An analysis of fault structures and seals is in progress to characterize the leakage potential that causes permeability variations and hydrostatic gradient in fluid pressure along each fault plane. Pressure gradient maps of the Upper and Middle Montney members within the study area are presented in Figure 5a and b. The overall trend of the pore pressure and the location of hydraulic discontinuities align with previously published results (Figure 3). Pore pressure and other petrophysical and mechanical properties in this study have been populated using kriging interpolation.

In addition to down-hole gauge measurements, all of the available drill stem test (DST) data were collected and the DST pore pressure from the overlying Halfway and Doig formations and the underlying Belloy Formation was mapped. Although DST is the most accurate source of pressure data it is not cost-effective to complete DSTs in the Montney Formation unconventional reservoir due to low permeability and low flow capacity, thus only the routine tests (PGFO, PGBU, SG) and DFITs are available. Figure 6 displays the DST pressure gradient map of the Halfway Formation, which is more uniform than the Montney Formation and generally remains close to the hydrostatic gradient (10 kPa/m) throughout the study area. Notably, a series of Halfway Formation conventional pools along the southern bounding fault of the Fort St. John graben is evident from the distribution of producing wells.

Minimum horizontal stress and fracture pressure gradient maps from the Lower Montney Member to the Doig Formation were also generated based on the DFIT reports and the data provided by operators. These two different datasets have the same mean values and lie within the same data range, and mixing the two datasets does not cause any sig-

nificant issues in stress analysis. Previous studies (Haghshenas and Qanbari, 2020) show that the tangent method, used in most DFIT interpretations, underestimates the actual fracture closure pressure (minimum horizontal stress [S_{Hmin}]). There is usually a 2–5% difference between the actual and measured values. This difference depends on the strength and average height of the asperities on the fracture walls. Therefore for stress modelling and HF simulation projects, correction to S_{Hmin} should be applied. Considering the absolute error in the S_{Hmin} estimation, this amount of error might be negligible, but the error is much more significant in fracture net pressure.

Pressure Difference and Seismicity Near the Suspended Well

When the November 30, 2018, earthquake sequence was initiated, zipper-HF was being carried out in two Lower–Middle Montney member wells (G and H), which was subsequently suspended. Over a two-week period (3 days before and 10 days after the November 30, 2018, mainshock), almost 600 events (M_L –0.3 to 4.5) were identified (Salvage and Eaton, 2021). Events appear tightly clustered, both spatially and in depth. Focal mechanism analysis suggests that this region of seismic activity is located within a transitional stress regime, with a mixture of reverse and strike-slip faulting over a small spatial extent (Salvage and Eaton, 2021). Figure 7 shows relocated seismic event hypocentres for the epicentral location of the November 30, 2018, earthquake sequence. A possible scenario to explain the observed pattern of seismicity, which includes small strike-slip events between the two wells, is that fault slip along the pressure-terrane boundary occurred aseismically, triggering dynamic rupture at a slightly greater depth (e.g., Debolt Formation). This hypothesis is currently being evaluated.

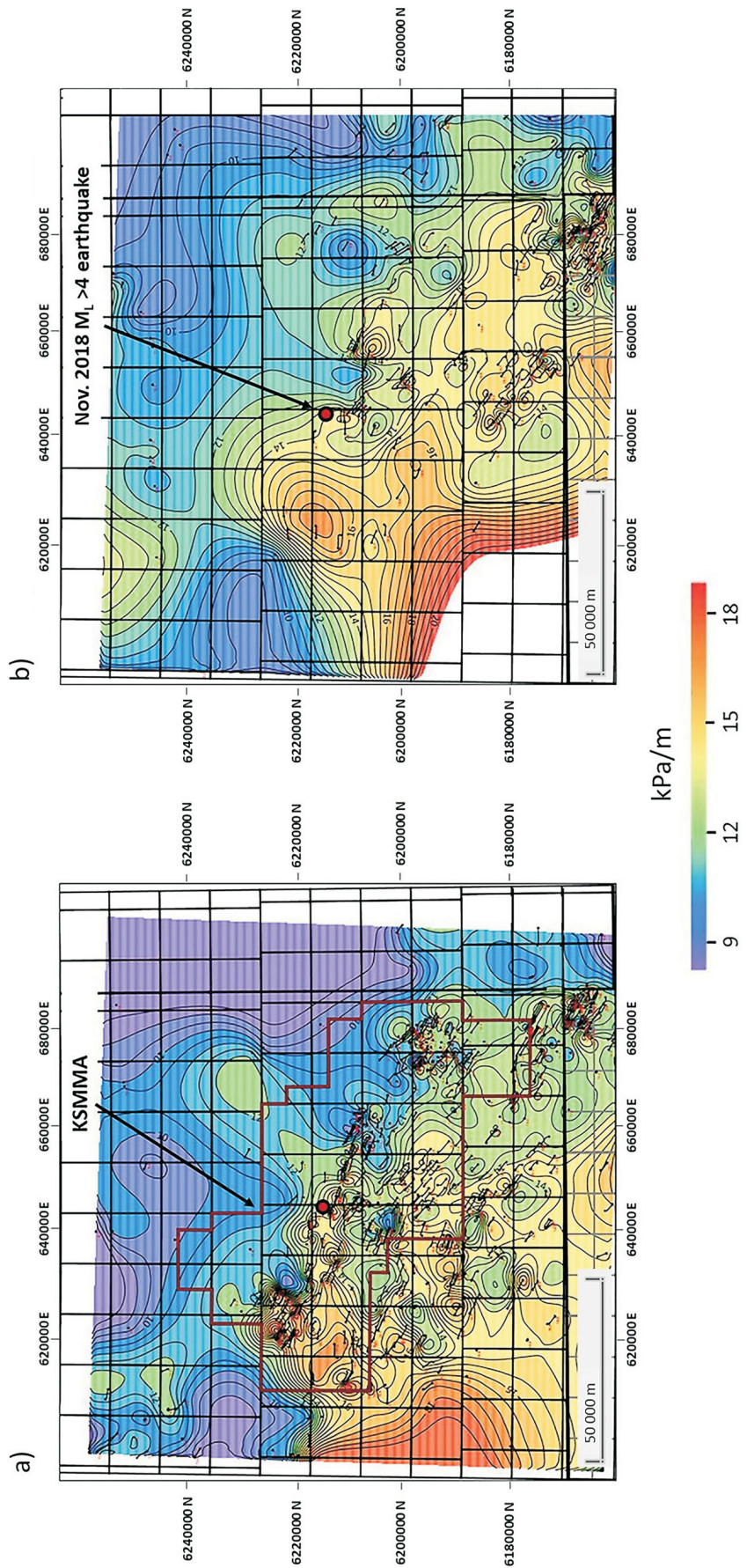


Figure 3. Pressure gradient (kilopascals per metre [kPa/m]) map of the **a)** Upper Montney and **b)** Middle Montney members of the Montney Formation (from Fox and Watson, 2019). Red circle shows the epicentral region of the local magnitude (M_L) 4.5 earthquake sequence, November 30, 2018. The earthquake location appears to correlate with significant lateral contrast in pore pressure gradient associated with the boundary between the Septimus High and the Tower Moderate Low pressure terranes (see Figure 2). Black symbols indicate well locations. All co-ordinates are in UTM Zone 10 North, NAD 83. Abbreviation: KSMIMA, Kiskatinaw Seismic Monitoring and Mitigation Area.

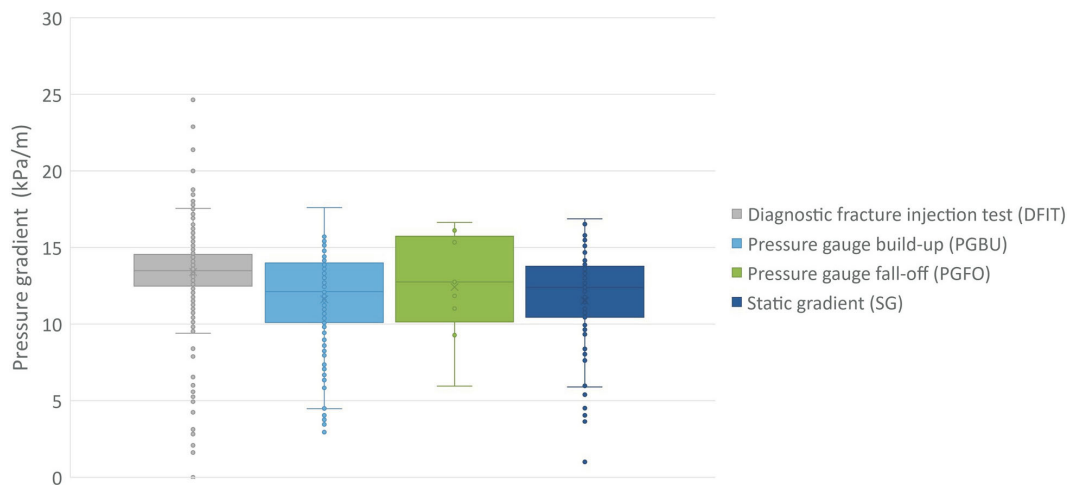


Figure 4. Box-and-whisker plot showing a comparison of pressure gradient data from different pressure measurement methods, compiled for the Montney Formation in this study. Abbreviation: kPa, kilopascal.

The initial static pressure of the G well was measured as approximately 38 MPa before the start of the HF operation. Following the earthquake sequence and for a period of about nine months, the formation pressures of the G well and the H well were measured as 35 and 28 MPa, respectively. The G well pressure drop of 3 MPa seems to be due to fluid leak-off into a nearby fault over the nine-month time interval. Also, the 10 MPa pressure difference between the two wells confirms the presence of a fault. It should be noted that H well is completed 47 m above the G well but this small difference in depth cannot cause such a large pressure difference. Also, based on close examination, the high pressure of the G well does not seem to be influenced by the fluid-injection pressure of the adjacent wells (<500 m distance), since no other nearby well shows abnormal pressure. Based on regional pore pressure gradient data, an extended normal fault (see ‘Property Modelling’ section, Figure 10) divides the entire study area into low- and high-pressure regions. The G and H wells are located in the high-pressure and low-pressure regions, respectively. Figure 8 demonstrates the pressure behaviour of the two wells before and after the November 30, 2018, earthquake. The pressure behaviour of these wells supports the fault-valve theory. Sibson (1990) introduced the concept of fault-valve theory, where a reactivated fault plane can act as an open valve for fluids, promoting leakage and causing a hydrostatic gradient in fluid pressure. This fluid pressure cycling may significantly increase the variations in fault strength. Changes in frictional strength over the interseismic period resulting from the fault-valve activity may substantially exceed the shear stress drop at failure. In such circumstances, recurrence intervals between successive events can be highly variable. In regions where large ruptures tend to nucleate, the largest fluid pressure fluctuations result from faults that remain active as a consequence of fluid overpressure. Geological evidence suggests that valve action may be especially important in the lower re-

gions of a seismogenic zone due to severely misoriented faults in the prevailing stress field. The most extreme fault-valve action is likely to be associated with high-angle reverse faults (Sibson, 1992). When fluid flow reactivates faults in the form of aseismic slip or earthquakes, the resulting shear deformation can cause considerable enhancement of the hydraulic diffusivity (in some cases, one order of magnitude increase). As mentioned earlier, the epicentre of the November 30, 2018, M_L 4.5 mainshock strongly correlates with a significant lateral pore pressure difference. Similar behaviour is observed in some other wells in the study area. Observations suggest a relationship between pressure difference across the fault and the induced seismicity in the vicinity of HF operations. The higher the pressure difference and the smaller the depth offset between the two wells, the greater the seismicity rate and magnitude. It is also expected that this pressure difference will affect the efficiency of HF jobs and the geometry of the fractures. Detailed studies are underway to validate these observations through numerical and statistical analysis.

Permeability Model

Permeability plays an important role in reservoir characterization since the distribution of permeable conduits within a reservoir controls fluid pressure diffusion (Riazi and Eaton, 2020). The most common permeability estimation methods are permeability prediction from core data, permeability calculation based on conventional well logs, and permeability estimation from the nuclear magnetic resonance (NMR) logs (Di, 2015). As the cost of cutting, running tests and analyzing the core data is nearly 10 times greater than well log analysis (Yao and Holditch, 1993), many attempts have been made to find permeability predictors in well logs. One of the most common approaches is using permeability–porosity correlations. These correlations are widely used in the industry and are suitable for quick

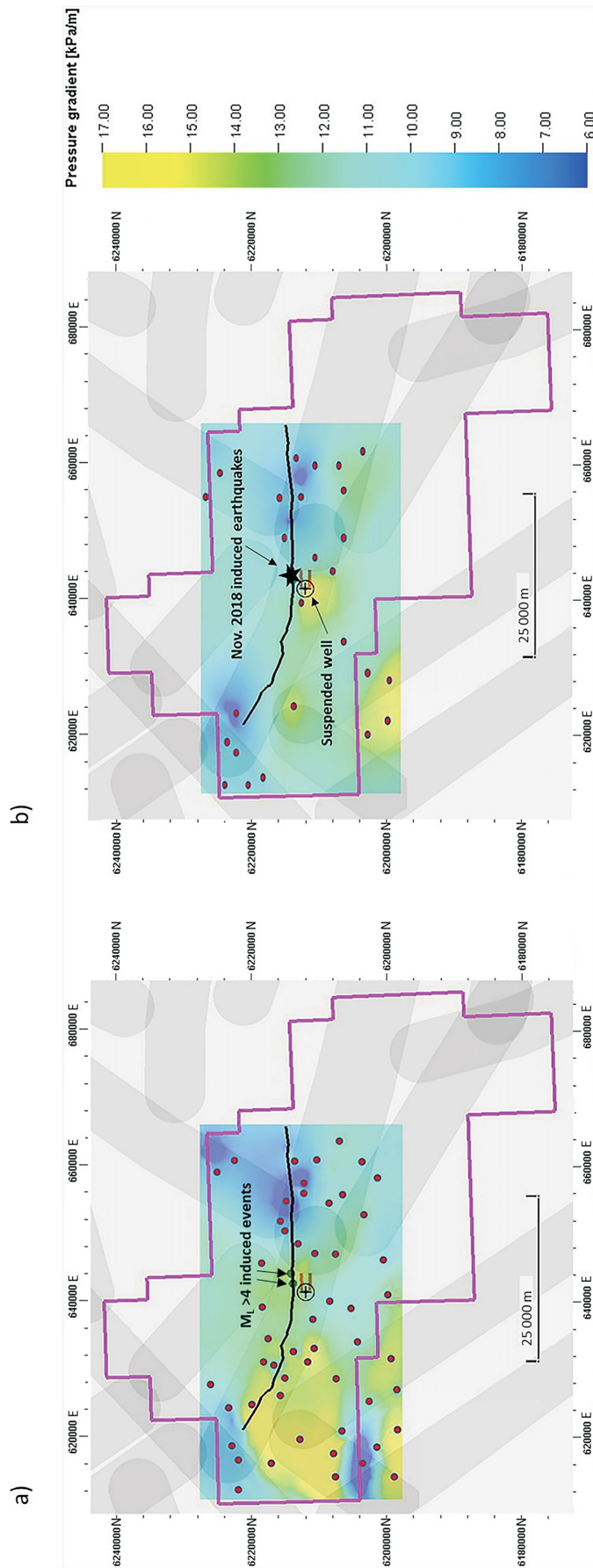


Figure 5. Pressure-gradient (kilopascals per metre [kPa/m]) maps of the **a)** Upper Montney and **b)** Middle Montney members based on data compiled in this study and populated using kriging interpolation. Data provided by geOLOGIC systems Ltd. © 2021. Red dots show the distribution of pressure data points in the model. The star is the epicentre of the November 30, 2018, main-shock and the black line represents the southern bounding fault (projected to the surface from the Deboit Formation) of the Fort St. John graben. Magenta outline shows the Kiskatinaw Seismic Monitoring and Mitigation area. The suspended well symbol marks the pad location of the two horizontal wells (orange lines) in Figure 7. Structural corridors are indicated by translucent shading (see Figure 2). All co-ordinates are in UTM Zone 10 North, NAD 83.

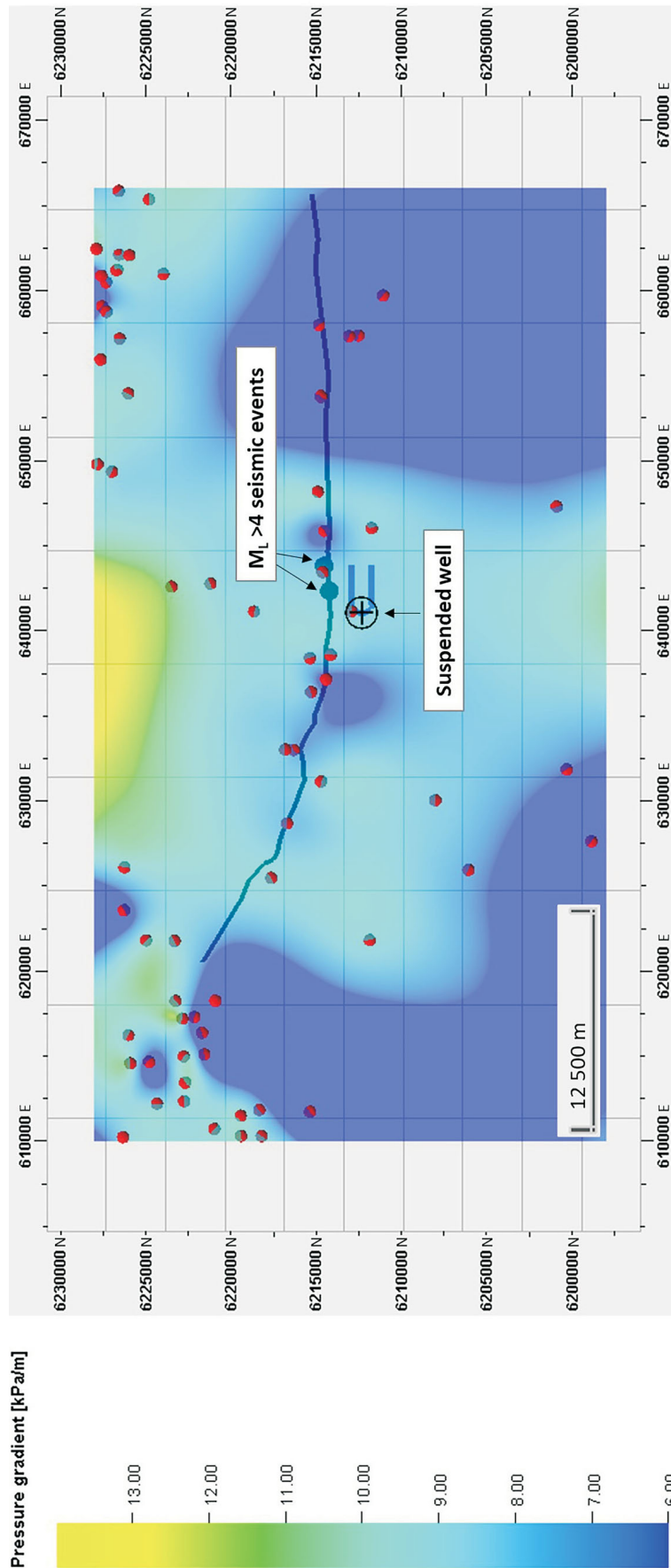


Figure 6. Pressure-gradient (kilopascals per metre [kPa/m]) map of the Halfway Formation, based on drill stem tests (DSTs). Red and grey dots show the locations of wells with pressure data. Data provided by geoLOGIC systems ltd. © 2021. The Halfway Formation overlies the Montney Formation but, unlike the Montney Formation, the Halfway Formation pore pressure gradient remains close to the hydrostatic gradient (10 kPa/m) throughout the study area. The southern bounding fault (projected to the surface from the Debolt Formation) of the Fort St. John graben is shown as the dark blue line. A number of conventional (structurally trapped reservoirs) producing wells are situated along the FS-JG fault, providing independent validation of the fault location and upward deformation into the Halfway Formation. The suspended well symbol marks the pad location of the two horizontal wells (light blue line) in Figure 7. All co-ordinates are in UTM Zone 10 North, NAD 83. Abbreviation: M_L , local magnitude.

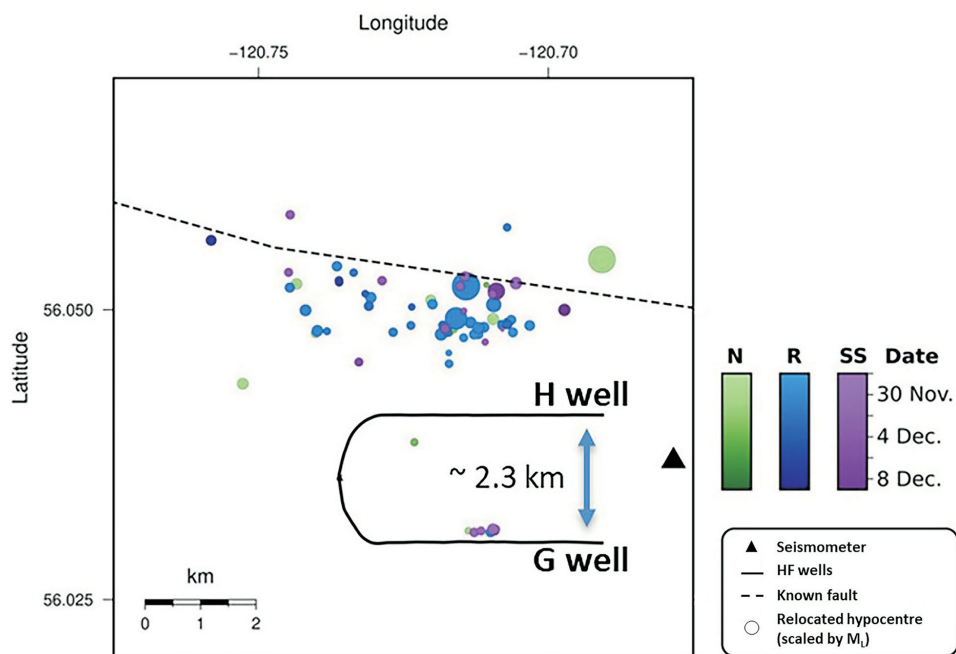


Figure 7. Epicentral location of the November 30, 2018, earthquake sequence coloured by type of event and shaded by timing of the event. The approximate location of the southern bounding fault (projected to the surface from the Debolt Formation) of the Fort St. John graben is shown by the dashed black line. Normal (N), reverse (R) and strike-slip (SS) mechanisms are shown by different colours. Figure is modified from Salvage and Eaton (2021). Abbreviations: HF, hydraulic fracturing; M_L , local magnitude.

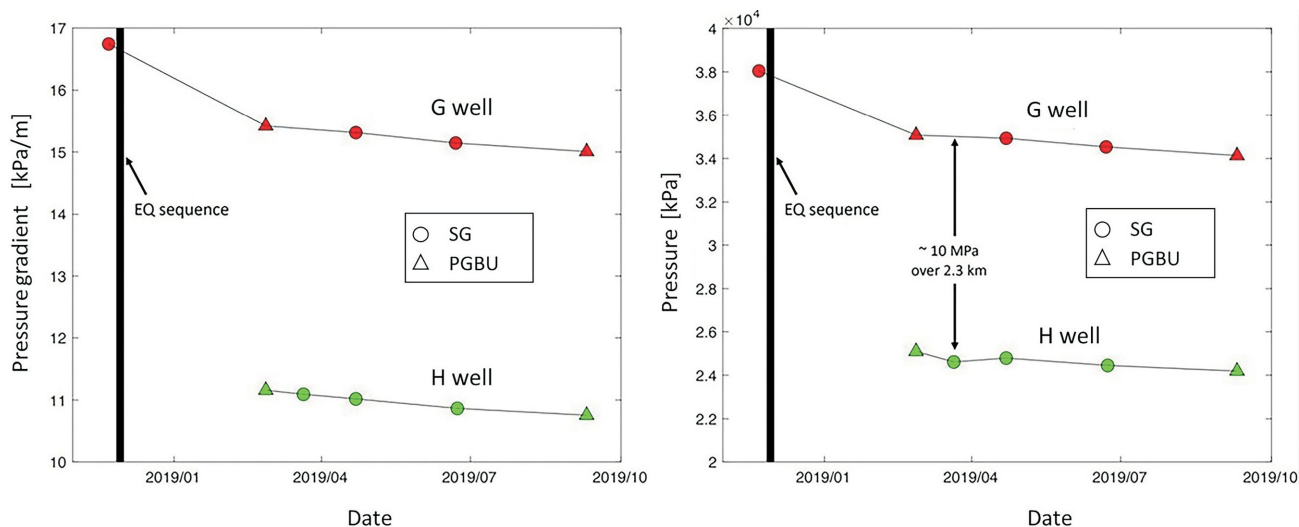


Figure 8. a) Bottom-hole pressure gradient and **b)** bottom-hole pressure for the G and H wells before and after the November 30, 2018, earthquake (EQ) sequence. There is an approximately 10 megapascal (MPa) pressure difference between the two wells, providing a tight constraint on the boundary between the Septimus High and Tower Moderate Low pressure terranes at this location (Figure 2). An apparent 3 MPa pressure drop after the mainshock may be related to fluid leak-off along the fault as predicted by the fault-valve model. Abbreviations: SG, static gradient test; PGBU, pressure gradient build-up test.

and still acceptable permeability estimation. For this study, the correlation used was

$$k = A\phi^a$$

where k is permeability (m^2), A is an empirical constant, ϕ is fractional porosity and a is a porosity exponent. The coeffi-

cient and the exponent were calibrated with core data. Since there are many well logs in the study area, detailed porosity and permeability distribution maps were produced. The resulting permeability maps correlate well with the structural corridors (Figure 9). Permeabilities derived from DFIT reports, DSTs and core analysis were also used

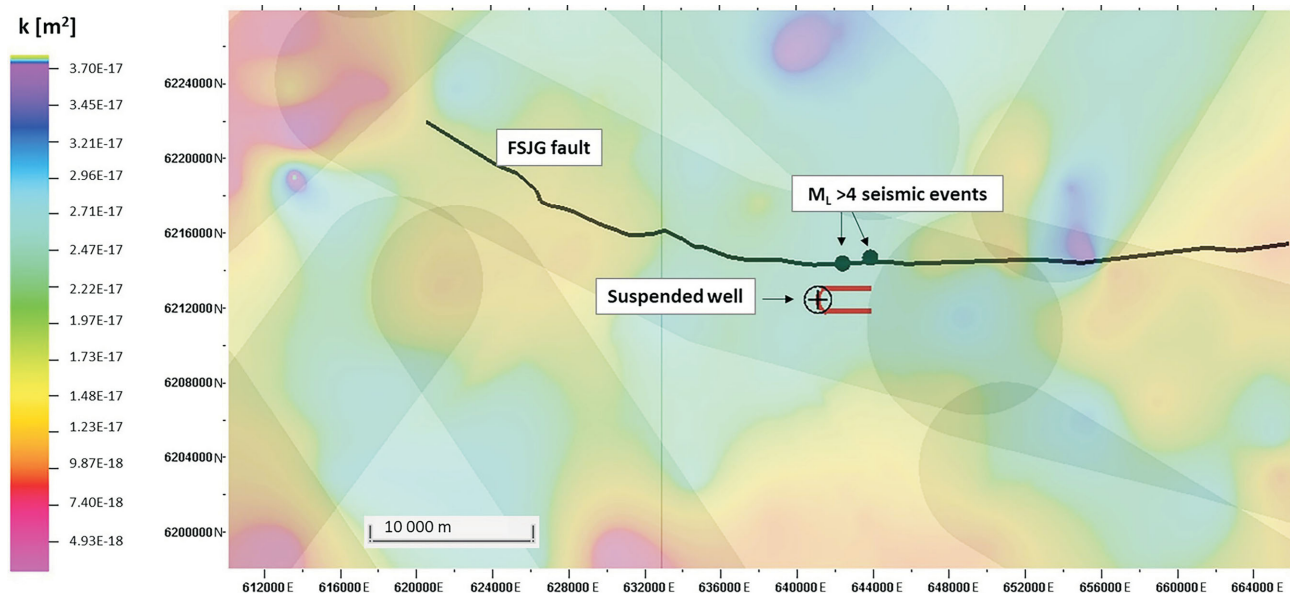


Figure 9. The Lower Montney Member permeability (k) map based on data compiled in this study using kriging interpolation. Data provided by geoLOGIC systems ltd. © 2021. Green dots show the locations of large magnitude events including the November 30, 2018, local magnitude (M_L) 4.5 mainshock. The green line represents the southern bounding fault of the Fort St. John graben (FSJG). The suspended well symbol marks the pad location of the two horizontal wells (red line) in Figure 7. Permeability shows a correlation with the structural corridors (indicated by translucent shading; see Figure 2). All co-ordinates are in UTM Zone 10 North, NAD 83.

for calibration. Log-derived permeabilities span a similar range of values.

Property Modelling

Well logs are arguably the best source of data for reservoir characterization and estimation of petrophysical properties at the macro scale. They can also be used to estimate dynamic elastic parameters, such as Poisson’s ratio and Young’s modulus. From more than 500 full suites of well logs, 100 wells were selected that had the best data quality and included (to the extent possible) the interval from the Debolt to Doig formations. An attempt was also made to have a relatively uniform distribution of well logs across the model area and a balance of locations across each fault. Logs used in this study included gamma-ray (GR), calliper (CAL), bulk density (RHOB, RHOZ), neutron and density porosity of sandstone (NPOR, DPFI), spontaneous potential (SP), photoelectric factor (PEF), shear and compressional sonic (DTS, DTP), shallow, medium and deep resistivity (Rxo, Rm, RD), and temperature (TEMP). Before log upscaling and property modelling, careful data cleaning and variogram analyses were performed for each zone to fit the best model based on the spatial correlation of the log samples. Petrophysical modelling was then carried out using the kriging interpolation method. To determine elastic rock properties in this study area, the following relationships were used for dynamic elastic moduli (Vishkai et al., 2017):

$$G_{dyn} = \text{dynamic shear modulus} = \frac{\rho_b}{\Delta t_s^2}$$

$$K_{dyn} = \text{dynamic bulk modulus} = \frac{\rho_b}{\Delta t_p^2} - \frac{4}{3} G_{dyn}$$

$$E_{dyn} = \text{dynamic Young's modulus} = \frac{9G_{dyn}K_{dyn}}{G_{dyn} + 3K_{dyn}}$$

$$\nu_{dyn} = \text{dynamic Poisson's ratio} = \frac{\frac{1}{2} \left(\frac{\Delta t_s}{\Delta t_p} \right)^2 - 1}{\left(\frac{\Delta t_s}{\Delta t_p} \right)^2 - 1}$$

where ρ_b is bulk density (kg/m^3) and Δt_s and Δt_p are shear and compressional slowness ($\mu\text{s/m}$), respectively.

Faults are the most likely explanation for hydraulic disconnections. Structural discontinuities can impact the sedimentation processes, reflected in the dislocation of reservoir properties along the faults. Low diffusivity and transmissibility of the faults also result in sharp contrasts in hydraulic properties, such as pressure and permeability. The discontinuities in permeability, Young’s modulus and the P-wave impedance, among other reservoir properties, show good correlation with the structural discontinuities. In areas with insufficient pressure data, the distribution of petrophysical and mechanical properties can help to infer the possible locations of the faults. Stratigraphic cross-sections and depth variations were inspected to confirm the location of a number of otherwise subtle faults (Figure 10).

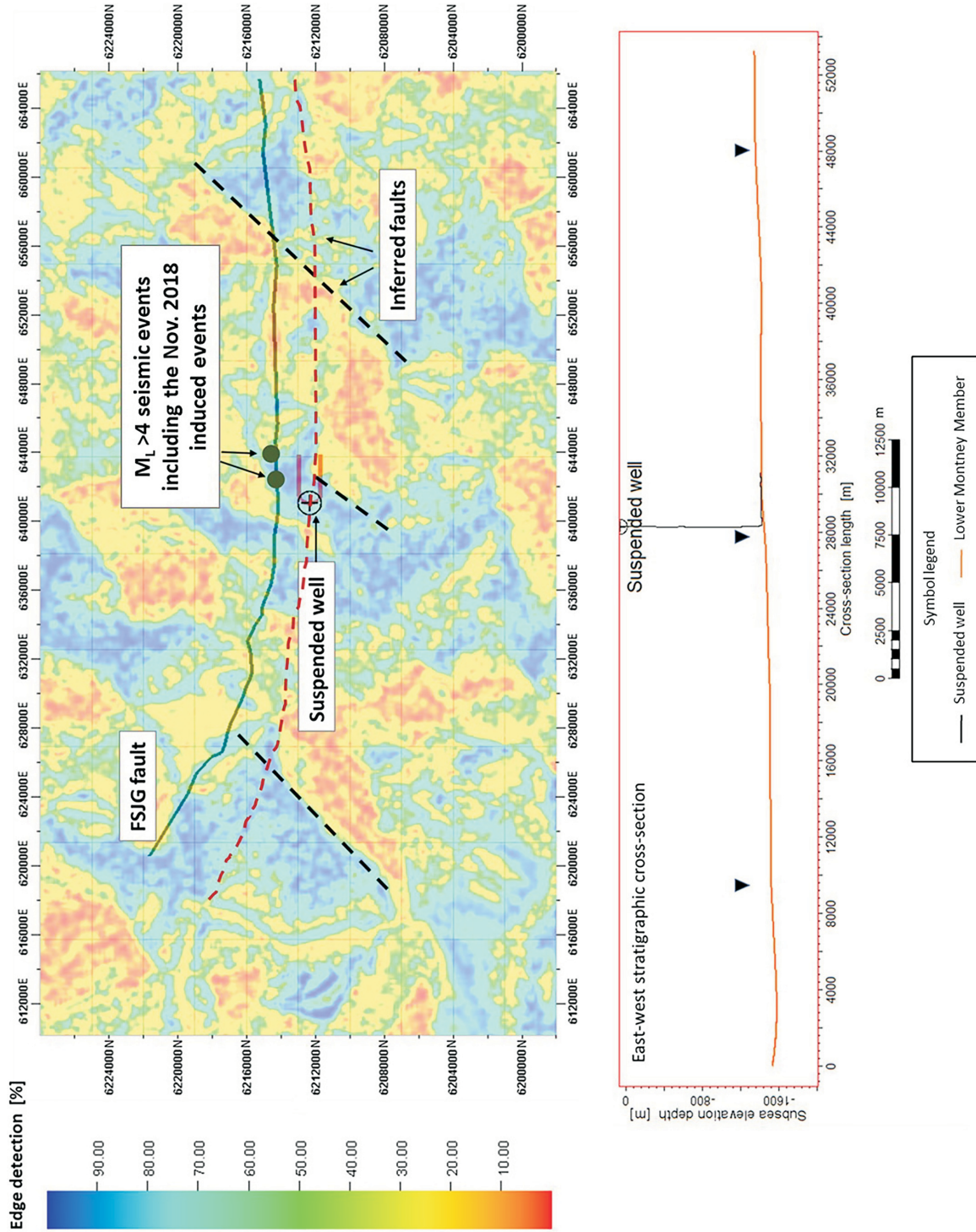


Figure 10. The Lower Montney Member edge detection map, expressed as a percent likelihood, based on log-derived Young's modulus. Data provided by geol.OGIC systems ltd. © 2021. Dashed lines are inferred faults based on property discontinuities. The inferred fault, shown as a red dashed line, correlates with a significant difference in the regional pore pressure gradient. The east-west stratigraphic cross-section (lower panel) shows the locations of these possible subtle faults. The suspended well symbol marks the pad location of the two horizontal wells (orange line) in Figure 7. All co-ordinates are in UTM Zone 10 North, NAD 83. Abbreviations: FSJG, Fort St. John graben; M_L, local magnitude.

Edge evidence is a statistical interpretation method in Schlumberger's Petrel, which can be used to enhance edges such as faults and salt body borders. It can detect sharp and/or fuzzy edges, whether short or long. This attribute can be used to enhance faults or the outline of geobody borders, if there is a suitable 'border' attribute that can be used as input. The edge evidence attribute searches locally in all directions for line segments where the values on the line differs significantly from the surrounding values. The result of the method is the best evidence of a line passing through that point. The better the evidence of a line, the higher the output value.

Conclusions

This compilation and other recent studies show that sealing faults act partially as pressure barriers, but seal preservation depends on the depth and reservoir pressure distribution. Observations suggest a relationship between the pressure difference across the fault and the induced seismicity rate and magnitude. The higher pressure difference seems to be correlated with higher seismicity rates and larger magnitudes. Also, variations in permeability and mechanical properties lie within the boundaries of structural corridors. In areas where pressure data are insufficient, the distribution of petrophysical and mechanical properties can help infer the locations of the possible faults.

Acknowledgments

This work was funded by a Natural Sciences and Engineering Research Council of Canada's Alliance grant and a scholarship from Geoscience BC. The authors would like to thank the BC Oil and Gas Commission and Geoscience BC for providing data; Schlumberger Canada Limited for the Petrel software platform; Itasca Consulting Group, Inc. for 3DEC™ software; and Halliburton Energy Services for GOHFER® software licensing. geoLOGIC systems ltd. is thanked for their contribution of data and software used in this study. All geoLOGIC systems ltd. data and geoSCOUT software is ©2021. Canadian Natural Resources Limited generously provided diagnostic fracture injection test data. The authors appreciate their peer reviewer, C. Wang, for taking the time and effort necessary to provide insightful guidance. All sponsors of the Microseismic Industry Consortium are thanked for their financial support.

References

Di, J. (2015): Permeability characterization and prediction in a tight oil reservoir, Edson Field, Alberta; M.Sc. thesis, University of Calgary, 113 p.

Enlighten Geoscience Ltd. (2021): Pressure, stress and fault slip risk mapping in the Kiskatinaw Seismic Monitoring and Mitigation Area, British Columbia; report prepared for the BC Oil and Gas Research and Innovation Society, Final Report ER-Seismic-2020-01, 81 p.

Fox, A.D. and Watson, N.D. (2019): Induced seismicity study in the Kiskatinaw Seismic Monitoring and Mitigation Area, British Columbia; report prepared for the BC Oil and Gas Commission, 51 p., URL <<https://www.bcogc.ca/files/reports/Technical-Reports/final-report-enlighten-geoscience-kssma-phase-1-study-2019w-appendices-links.pdf>> [November 2021].

Haghshenas, B. and Qanbari, F. (2020): Field-wide review of diagnostic fracture injection tests DFIT in Montney and Duvernay formations—part 1: stress and pressure distributions; Society of Petroleum Engineers Canada, Unconventional Resources Conference, September 28–October 2, 2020, virtual, paper no. SPE-199990-MS.

Riazi, N. and Eaton, D.W. (2020): Anatomy of a buried thrust belt activated during hydraulic fracturing; *Tectonophysics*, v. 795, art. 228640.

Salvage, R. and Eaton, D. (2021): How is induced seismicity affected by transitional stress regimes?; American Rock Mechanics Association, 55th U.S. Rock Mechanics Geomechanics Symposium, June 18–25, 2021, virtual, paper no. ARMA-2021-2078.

Sibson, R. (1992): Implications of fault-valve behaviour for rupture nucleation and recurrence; *Tectonophysics*, v. 211, no. 1–4, p. 283–293.

Sibson, R.H. (1990): Conditions for fault-valve behaviour; *in* Deformation Mechanisms, Rheology and Tectonics, R.J. Knipe and E.H. Rutter (ed.), Geological Society, Special Publication no. 54, p. 15–28.

Vishkai, M., Wang, J., Wong, R.C., Clarkson, C.R. and Gates, I.D. (2017): Modeling geomechanical properties in the Montney Formation, Alberta, Canada; *International Journal of Rock Mechanics and Mining Sciences*, v. 96, p. 94–105.

Visser, R., Smith, B., Kao, H., Babaie Mahani, A., Hutchinson, J. and McKay, J.E. (2017): A comprehensive earthquake catalogue for northeastern British Columbia and western Alberta, 2014–2016; Geological Survey of Canada, Open File 8335, 28 p.

Wood, J.M., Euzen, T., Sharp, L. and Leroux, S. (2021): Phase separation and secondary migration of methane rich gas accompanying uplift of an unconventional tight hydrocarbon system, Montney Formation, western Canada; *Marine and Petroleum Geology*, v. 124, art. 104808.

Wozniakowska, P., Eaton, D., Deblonde, C., Mort, A. and Ardakani, O. (in press): Identification of regional structural corridors in the Montney play using trend surface analysis combined with geophysical imaging; Geological Survey of Canada, Open File Report, OF-8814, 59 p.

Yao, C. and Holditch, S. (1993): Estimating permeability profiles using core and log data; Society of Petroleum Engineers, Eastern Regional Meeting, November 2–4, 1993, Pittsburgh, Pennsylvania, paper no. SPE-26921-MS.